Humanized *H19/Igf2* locus reveals diverged imprinting mechanism between mouse and human and reflects Silver–Russell syndrome phenotypes

Stella K. Hur[a], Andrea Freschi[b], Folami Ideraabdullah[c], Joanne L. Thorvaldsen[a], Lacey J. Luense[a], Angela H. Weller[a], Shelley L. Berger[a], Flavia Cerrato[b,1], Andrea Riccio[b,d,1], and Marisa S. Bartolomei[a,1]

[a]Department of Cell and Developmental Biology, University of Pennsylvania Perelman School of Medicine, Philadelphia, PA 19104; [b]Department of Environmental, Biological, and Pharmaceutical Sciences and Technologies, Second University of Naples, 81100 Caserta, Italy; [c]Department of Genetics, University of North Carolina at Chapel Hill, Chapel Hill, NC 27599; and [d]Institute of Genetics and Biophysics A. Buzzati-Traverso, 80131 Naples, Italy

Edited by Shirley Tilghman, Princeton University, Princeton, NJ, and approved July 14, 2016 (received for review February 24, 2016)

Genomic imprinting affects a subset of genes in mammals, such that they are expressed in a monoallelic, parent-of-origin–specific manner. These genes are regulated by imprinting control regions (ICRs), *cis*-regulatory elements that exhibit allele-specific differential DNA methylation. Although genomic imprinting is conserved in mammals, ICRs are genetically divergent across species. This raises the fundamental question of whether the ICR plays a species-specific role in regulating imprinting at a given locus. We addressed this question at the *H19/insulin-like growth factor 2* (*Igf2*) imprinted locus, the misregulation of which is associated with the human imprinting disorders Beckwith–Wiedemann syndrome (BWS) and Silver–Russell syndrome (SRS). We generated a knock-in mouse in which the endogenous *H19/Igf2* ICR (mIC1) is replaced by the orthologous human ICR (hIC1) sequence, designated $H19^{hIC1}$. We show that hIC1 can functionally replace mIC1 on the maternal allele. In contrast, paternally transmitted hIC1 leads to growth restriction, abnormal hIC1 methylation, and loss of *H19* and *Igf2* imprinted expression. Imprint establishment at hIC1 is impaired in the male germ line, which is associated with an abnormal composition of histone posttranslational modifications compared with mIC1. Overall, this study reveals evolutionarily divergent paternal imprinting at IC1 between mice and humans. The conserved maternal imprinting mechanism and function at IC1 demonstrates the possibility of modeling maternal transmission of hIC1 mutations associated with BWS in mice. In addition, we propose that further analyses in the paternal knock-in $H19^{+/hIC1}$ mice will elucidate the molecular mechanisms that may underlie SRS.

genomic imprinting | DNA methylation | H19 | IGF2 | Silver–Russell syndrome

Genomic imprinting is a conserved, epigenetic process in mammals that regulates the expression of a small number of genes in a monoallelic, parent-of-origin–specific manner. Typically clustered within domains, the parental-specific expression of imprinted genes is controlled by a *cis*-regulatory element, the imprinting control region (ICR). During gametogenesis, ICRs acquire differential DNA methylation patterns according to the sex of the germ cells. This DNA methylation is maintained in somatic cells after fertilization but is erased in primordial germ cells, allowing the establishment of sex-specific imprints in mature gametes. The proper establishment, maintenance, and erasure of imprints are crucial for the correct expression of imprinted genes. Misregulation of imprinted genes is associated with human imprinting disorders, including Beckwith–Wiedemann syndrome (BWS), an overgrowth disorder, and Silver–Russell syndrome (SRS), an undergrowth disorder (1–3).

Mouse models have been valuable to the study of imprinting at the *H19/insulin-like growth factor 2* (*Igf2*) locus, serving as a proxy for the orthologous human locus. On distal mouse chromosome 7, reciprocal imprinting of the paternally expressed fetal growth factor gene, *Igf2,* and the maternally expressed noncoding RNA, *H19,* is regulated by the ICR located between *H19* and *Igf2*, herein termed imprinting center 1 (IC1) (4). IC1 is hypomethylated in female germ cells and forms a CCCTC-binding factor (CTCF)-dependent insulator in somatic cells, preventing the interaction of the *Igf2* promoters with downstream enhancers that are shared between *H19* and *Igf2*. CTCF binding at the maternal IC1 is critical for maintaining its methylation-free status and silencing *Igf2* expression (5). In contrast, IC1 DNA methylation is acquired during spermatogenesis. Methylation at IC1 blocks CTCF binding and allows *Igf2* expression.

Comparative genome studies have revealed extensive conservation of *H19/Igf2* in therians (6). Consistently, key features of imprinting, as well as spatial organization of the mouse and human loci, are shared, including DNA methylation patterns, CTCF-binding sites (CTSs), and *cis*-regulatory elements. Notably, however, the length of IC1 and the number of CTSs within IC1 have diverged; the ∼5-kb human IC1 has seven CTSs, whereas the corresponding mouse sequence is ∼2 kb and has four CTSs. In addition, with the exception of the CTCF-binding motifs, IC1 exhibits low sequence homology between mice and humans (7, 8). This raises the question of whether the human IC1 sequence could successfully regulate *H19/Igf2* imprinting in the mouse. If it can, then an in vivo model for imprinting disorders associated with mutations at human IC1 could be generated (9).

Significance

Genomic imprinting is essential for mammalian development. Curiously, elements that regulate genomic imprinting, the imprinting control regions (ICRs), often diverge across species. To understand whether the diverged ICR sequence plays a species-specific role at the *H19/insulin-like growth factor 2* (*Igf2*) imprinted locus, we generated a mouse in which the human ICR (hIC1) sequence replaced the endogenous mouse ICR. We show that the imprinting mechanism has partially diverged between mouse and human, depending on the parental origin of the hIC1 in mouse. We also suggest that our mouse model is optimal for studying the imprinting disorders Beckwith–Wiedemann syndrome when hIC1 is maternally transmitted, and Silver–Russell syndrome when hIC1 is paternally transmitted.

Author contributions: S.K.H., A.F., F.I., J.L.T., F.C., A.R., and M.S.B. designed research; S.K.H., A.F., F.I., J.L.T., L.J.L., and A.H.W. performed research; S.L.B. contributed new reagents/analytic tools; S.K.H., J.L.T., and M.S.B. analyzed data; and S.K.H., F.C., A.R., and M.S.B. wrote the paper.

The authors declare no conflict of interest.

This article is a PNAS Direct Submission.

[1]To whom correspondence may be addressed. Email: flavia.cerrato@unina2.it, andrea.riccio@igb.cnr.it, or bartolom@mail.med.upenn.edu.

This article contains supporting information online at www.pnas.org/lookup/suppl/doi:10.1073/pnas.1603066113/-/DCSupplemental.

Although interspecies compatibility of human IC1 was previously investigated in a transgenic mouse model (8), the human transgene failed to exhibit the expected imprinting pattern. The transgene acquired DNA methylation in male germ cells in a copy number-dependent manner, but the imprint was not stably maintained in somatic cells. In addition, the human *H19* transgene was abnormally expressed on paternal transmission. Interpretation of these observations is complicated by transgene copy number variation, however. Furthermore, because long-range chromatin looping plays an essential role in *H19/Igf2* imprinting (10, 11), the transgene insertion site may influence the phenotype. Thus, it is imperative to test the functionality of the human IC1 element at the orthologous locus.

Here we generated a knock-in mouse model in which the endogenous mouse IC1 (mIC1) was replaced by human IC1 (hIC1). Our goal was to investigate the extent to which hIC1 can functionally replace mIC1. We found that hIC1 properly recapitulates mIC1 function on the maternal allele, whereas hIC1 fails to properly regulate the *H19/Igf2* locus on the paternal allele. hIC1 is incompletely methylated in the male germ cells of knock-in mice, which is associated with increased enrichment of dimethylation of histone H3 at lysine 4 (H3K4me2) on hIC1. Overall, this study reveals interspecies incompatibility of hIC1 in the mouse male germ line. Importantly, we show that abnormal histone modification composition at hIC1 may affect the proper establishment of DNA methylation at hIC1 during mouse germ cell development.

Results

Generation of the $H19^{hIC1}$ Allele. To determine whether hIC1 could functionally substitute for the orthologous mouse sequence, we replaced the endogenous mIC1 with hIC1 by gene targeting in embryonic stem (ES) cells (Fig. 1*A*). Even though we obtained highly chimeric mice after blastocyst injection of the targeted ES cells, germline transmission of the targeted allele was inefficient. Only one female pup with the $H19^{hIC1}$ allele was live-born out of >250 agouti pups; all other agouti pups were wild-type, suggesting that the pups inheriting the $H19^{hIC1}$ allele might be dying prenatally. The single live-born female knock-in pup was of noticeably smaller size compared with its wild-type siblings and remained small.

The neomycin resistance cassette (NeoR) was excised by crossing the female to EIIA-Cre male on a C57BL/6J (B6) background (Jackson Laboratories). Germ-line transmission of the targeted allele and excision of NeoR were confirmed by Southern blot analysis (Fig. 1*B*). When bred to a B6 male, the female knock-in mouse was fertile, and wild-type and knock-in progeny were born in the expected Mendelian ratios with no sex bias. Embryonic lethality on paternal transmission was again observed after NeoR excision. The use of knock-in males in a B6/CF1 mixed strain for paternal transmission did not resolve the embryonic lethality. These results rule out NeoR and pure B6 background as being solely responsible for the failure to obtain mutant pups. The $H19^{hIC1}$ allele was maintained through maternal transmission in a B6 background.

The Maternally Transmitted $H19^{hIC1}$ Allele Can Functionally Substitute for mIC1. To investigate *H19* and *Igf2* imprinting when the targeted allele was maternally transmitted, we bred female $H19^{hIC1/+}$ mice to B6 (CAST7) mice, which have a *Mus musculus castaneus* chromosome 7 on a B6 background (12). This cross allows the parental origin of *H19* and *Igf2* expression to be distinguished in F1 progeny. Heterozygous $H19^{hIC1/+}$ mice were compared with their wild-type littermates ($H19^{+/+}$). The $H19^{hIC1/+}$ and $H19^{+/+}$ mice were born in Mendelian ratios with no sex bias and no difference in neonatal weight (Fig. 2*A*). We assayed expression and IC1 methylation in neonatal livers, where *H19* and *Igf2* are highly expressed, and detected monoallelic expression in all cases (Fig. 2*B*). Consistently, total expression levels of *H19* and *Igf2* were statistically equivalent in $H19^{+/+}$ and $H19^{hIC1/+}$ livers, as measured by quantitative real-time PCR (qRT-PCR) (Fig. 2*C*).

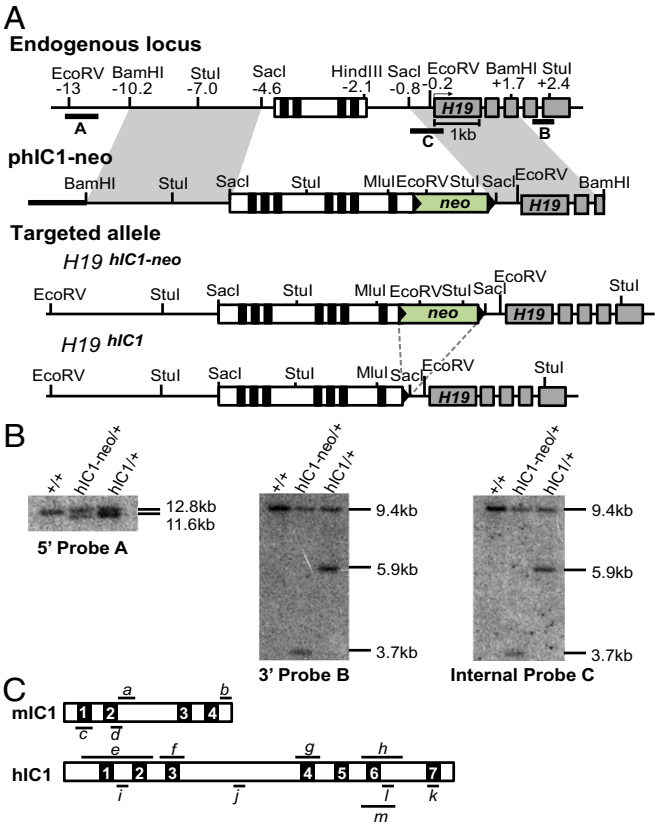

Fig. 1. Targeting strategy to generate the $H19^{hIC1}$ allele. (*A*) Schematics of the endogenous locus, targeting vector (phIC1-neo), correctly targeted allele ($H19^{hIC1\text{-}neo}$), and targeted allele after excision of the neoR cassette ($H19^{hIC1}$). Depicted are the IC1 (white rectangle) with CTCF-binding sites (black blocks within the IC1), *H19* exons (gray rectangles), pBluescriptIIKS sequence (bold line), neoR cassettes (green rectangles), loxP sites (black arrowheads), and endogenous mouse DNA (thin line). Restriction sites and their relative positions (in kb) to the *H19* transcription start sites are indicated above the endogenous locus. Probes (A, B, and C) used for Southern blot analyses are shown as thick lines below the endogenous locus. (*B*) Southern blot analysis to confirm correct targeting of the alleles. Genomic DNA from wild-type (+/+), hIC1-neo/+, and hIC1/+ mice was either digested with EcoRV-MluI and hybridized to external 5′ probe A or digested with StuI and hybridized to external 3′ probe B or to internal probe C. (*C*) Depiction of mIC1 (*Top*) and hIC1 (*Bottom*) highlighting regions analyzed by qRT-PCR (*a*–*m*). IC1s are illustrated in the orientation shown in *A*, with each CTS numbered. *a*, bisulfite treatment followed by sequencing for mIC1; *b* and *c*, ChIP–qRT-PCR for mIC1; *d*, pyrosequencing for mIC1; *e*–*h*, bisulfite treatment followed by sequencing for hIC1; *i*–*k*, ChIP–qRT-PCR for hIC1; *l*, pyrosequencing for hIC1; *m*, bisulfite treatment followed by sequencing for hIC1 (used for oocytes). Details are provided in *Materials and Methods*.

DNA methylation at hIC1 on the maternal allele and endogenous mIC1 on the paternal allele was measured by bisulfite mutagenesis of genomic DNA, followed by pyrosequencing. The maternal hICI was hypomethylated, as expected (Fig. 2*D*). Methylation at several other ICRs in $H19^{hIC1/+}$ livers was normal, suggesting that the general imprinting machinery is functioning normally (Fig. S1*A*). Finally, hIC1 was properly hypomethylated in the oocytes of $H19^{hIC1/+}$ females (Fig. 2*E*). We repeated these analyses in two sequential generations of the $H19^{hIC1}$ allele maternal transmission offspring and obtained the same results. Overall, these data illustrate that hIC1 can functionally replace mIC1 on the maternal allele.

The Paternally Transmitted $H19^{hIC1}$ Allele Leads to Abnormal Insulation at the *H19/Igf2* Locus. To investigate *H19* and *Igf2* imprinting on the paternal allele, we bred male $H19^{hIC1/+}$ mice to B6 (CAST7) mice.

GENETICS

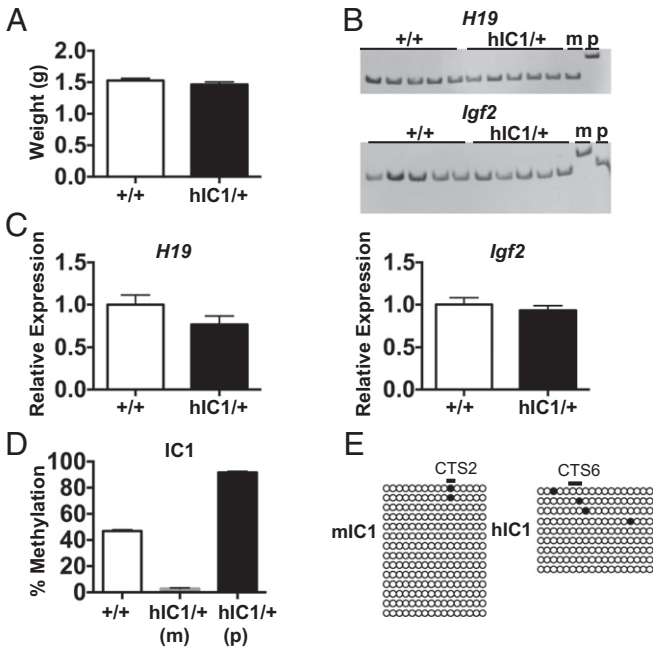

Fig. 2. Maternal transmission of the $H19^{hIC1}$ allele. (*A*) Neonatal (P0) weight of wild-type (+/+) and hIC1/+ mutant offspring. (*B*) Allele-specific expression of *H19* and *Igf2* in neonatal liver analyzed by restriction fragment length polymorphism (RFLP). Genotypes (wild-type and hIC1/+) and maternal (m) and paternal (p) allele controls are indicated above each gel. (*C*) Total expression of *H19* and *Igf2* in neonatal liver analyzed by qRT-PCR. (*D*) Percent methylation at IC1 in neonatal liver measured by pyrosequencing. Maternal (m) and paternal (p) alleles in hIC1/+ are shown separately, because different primers were used. Assay *d* was used for the wild-type (+/+) and hIC1/+(p), and assay *l* was used for hIC1/+(m) (Fig. 1*C*). (*E*) IC1 methylation in oocytes analyzed by bisulfite treatment followed by sequencing. Assay *a* was used for mIC1, and assay *m* was used for hIC1 (Fig. 1*C*). Empty and filled circles indicate unmethylated and methylated cytosines in CG dinucleotides, respectively. Each horizontal row of circles denotes individual strands of cloned DNA. Cytosines in CG dinucleotides that are conserved between mouse and human and located within the CTS are depicted as black lines above the clones and marked as CTS2 and CTS6 (13). In *A* and *C*, two-tailed Student's *t* test with equal variance was used; no significant differences were observed. In *A*–*D*, wild-type (+/+), $n = 11$; hIC1/+, $n = 12$ (from three litters). Bars represent the mean ± SEM; error bars in *A* and *D* are too small to be visible on the graph.

All live-born neonates were wild-type, similar to what was observed when breeding for germ-line transmission in chimeric mice, suggesting that paternal transmission of the $H19^{hIC1}$ allele is embryonic lethal. To investigate this possibility, we isolated embryonic day (E)15.5 conceptuses. Although the $H19^{+/hIC1}$ conceptuses were viable, the $H19^{+/hIC1}$ embryos and placentas were smaller and weighed significantly less compared with those of $H19^{+/+}$ (Fig. 3*A*). Anecdotally, such a size difference was not apparent at E10.5, and a trend toward a smaller size was observed at E12.5. The fetal/placental weight ratio was not different between E15.5 $H19^{+/+}$ and $H19^{+/hIC1}$, demonstrating that $H19^{+/hIC1}$ tissues were proportionately smaller (Fig. S2*A*).

Allele-specific RNA analysis revealed biallelic *H19* in E15.5 $H19^{+/hIC1}$ livers and placentas, with equal expression derived from the two parental alleles (Fig. 3*B* and Fig. S2*D*), suggesting complete derepression of paternal *H19*. In contrast, paternal *Igf2* expression was barely detectable, indicating complete repression of *Igf2* (Fig. 3*B* and Fig. S2*D*). Consistently, qRT-PCR analyses revealed approximately 3.4-fold and 1.5-fold increases of *H19* in liver and placenta, respectively, and undetectable *Igf2* in $H19^{+/hIC1}$ compared with $H19^{+/+}$ embryos in both tissues (Fig. 3*C* and Fig. S2*E*). Similar results were observed in E9.5 whole embryos (Fig. S2 *B* and *C*).

We next examined the extent to which methylation at hIC1 correlated with abnormal expression in heterozygous livers and placentas. hIC1 was completely unmethylated on the paternal allele, resembling the endogenous mIC1 on the maternal allele (Fig. 3*D* and Fig. S2*F*). This unusual methylation pattern was not due to a gross defect in the methylation machinery, because methylation at other ICRs was normal in $H19^{+/hIC1}$ embryos (Fig. S1*B*).

Finally, to determine whether the hypomethylated state of hIC1 is associated with ectopic binding of CTCF on the paternal allele, we performed allele-specific chromatin immunoprecipitation (ChIP) followed by quantitative real-time PCR (ChIP–qRT-PCR) for CTCF in E12.5 mouse embryonic fibroblasts (MEFs). As expected, CTCF bound only to the unmethylated hIC1 on the maternal allele and did not bind to the methylated mIC1 on the paternal allele in $H19^{hIC1/+}$ MEFs. In contrast, CTCF bound to both the unmethylated mIC1 on the maternal allele and the unmethylated hIC1 on the paternal allele in $H19^{+/hIC1}$ MEFs (Fig. 3*E*). The results demonstrate that paternal hIC1 is unable to acquire or maintain the hypermethylated state of endogenous mIC1, fails to repress *H19*, and instead gains a CTCF-dependent insulator function.

Incomplete Establishment of Genomic Imprinting at hIC1 During Spermatogenesis. Because the paternal allele in E15.5 $H19^{+/hIC1}$ embryos was hypomethylated, we assayed DNA methylation at earlier stages (Fig. S3). We did not detect any methylation at hIC1 as early as the blastocyst stage, suggesting that either methylation was not established during spermatogenesis or methylation was established but was lost during preimplantation development (Fig. S3). To distinguish between these possibilities, we examined DNA methylation at hIC1 in sperm of $H19^{hIC1/+}$ males, and observed partial methylation (Fig. 4 *A* and *B*). As positive controls, we analyzed methylation at endogenous hIC1 in human sperm samples from two fertile men as well as at endogenous mIC1 in $H19^{hIC1/+}$ sperm and found that all were hypermethylated, as expected (Fig. 4 *A* and *B*).

To explore whether the methylation at hIC1 in $H19^{hIC1/+}$ sperm could be maintained after the first cleavage division, we assayed $H19^{+/hIC1}$ two-cell embryos in which the zygote had undergone one round of mitosis. We found reduced methylation levels (close to one-half less) at hIC1 in two-cell embryos compared with mature sperm (Fig. 4*A*). These results demonstrate that the DNA methylation is partially established at hIC1 during spermatogenesis, but is not maintained in preimplantation development.

Increased Enrichment of H3K4me2 at hIC1 in Spermatogenic Cells. To investigate factors that may inhibit complete establishment of DNA methylation at hIC1 during spermatogenesis, we examined histone posttranslational modifications at hIC1. Parental allele-specific histone modifications have been described at mIC1 in both somatic and germ cells (14–18). Several studies have suggested an antagonistic relationship between "activating marks," such as dimethylation and trimethylation of histone H3 at lysine 4 (H3K4me2 and H3K4me3, respectively), and DNA methylation (17–20). Other studies have shown a strong relationship between "repressive marks," such as trimethylation of histone H3 at lysine 9 (H3K9me3), and DNA methylation (21). In fact, H3K4 methylation is found preferentially on the hypomethylated maternal IC1, and H3K9me3 is found on the hypermethylated paternal IC1 in mouse and human somatic cells (11, 14). We hypothesized that depletion of H3K9me3, increased enrichment of H3K4me2, or both contribute to the inability to fully establish DNA methylation at hIC1.

Spermatogenic cells were fractionated by the STA-PUT method, and chromatin was isolated from a round spermatid-enriched fraction (22). ChIP–qRT-PCR analyses in round spermatids revealed that hIC1 had fivefold greater enrichment of H3K4me2

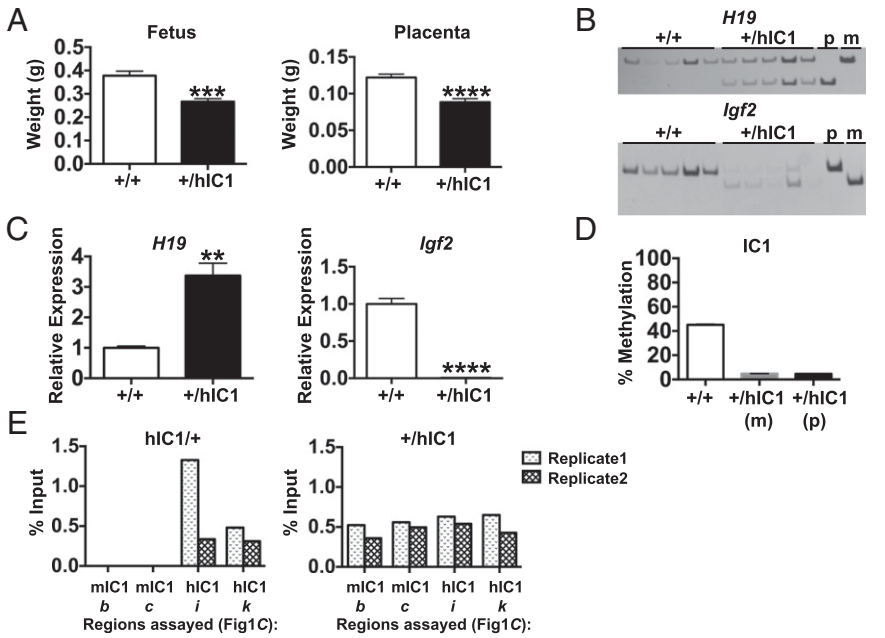

Fig. 3. Paternal transmission of the $H19^{hIC1}$ allele. (*A*) E15.5 fetal and placental weight of wild-type (+/+) and +/hIC1 mutant offspring. (*B*) Allele-specific expression of *H19* and *Igf2* in E15.5 livers analyzed by RFLP. PCR cycle numbers varied between wild-type (+/+) and +/hIC1 for *Igf2* (Table S1; see Table S2 for primers). (*C*) Total expression of *H19* and *Igf2* in E15.5 livers analyzed by qRT-PCR. (*D*) Percent methylation at IC1 in E15.5 livers measured by pyrosequencing. Assay *d* was used for wild-type (+/+) and +/hIC1(m), and assay *l* was used for +/hIC1(p) (Fig. 1*C*). (*E*) CTCF binding at mIC1 and hIC1 in heterozygous (hIC1/+ and +/hIC1) E12.5 MEFs analyzed by ChIP–qRT-PCR. Assays *b*, *c*, *i*, and *k* were used (Fig. 1*C*); results from two biological replicates are shown separately. The *y*-axis denotes percent input of CTCF IP normalized to nonspecific IgG (percent input of CTCF − percent input of IgG). $^{**}P < 0.01$; $^{***}P < 0.001$; $^{****}P < 0.0001$, two-tailed Student's *t* test with equal variance (*A*) or unequal variance (*C*). In *A*–*D*: wild-type (+/+), $n = 8$; +/hIC1, $n = 6$ (from two litters). Bars represent the mean ± SEM; error bars in *D* are too small to be seen on the graph.

compared with mIC1 (Fig. 4*C*). Unlike previous studies that did not report significant enrichment of H3K9me3 above background at mIC1 in the male germ line (14, 17), we obtained a ChIP signal above background. This discrepancy could be attributed to the different antisera used for H3K9me3. Nevertheless, there was no difference in the enrichment of H3K9me3 between hIC1 and mIC1. Our finding that the difference in H3K4me2 between mIC1 and hIC1 is greater than the difference in H3K9me3 suggests that (*i*) H3K9me3 does not affect the acquisition of DNA methylation at hIC1 during spermatogenesis, and (*ii*) enrichment of activating histone marks at hIC1 contributes in part to the incomplete establishment of imprinting at hIC1 during spermatogenesis (Fig. 4*C*).

Abnormal Placental Morphology in $H19^{+/hIC1}$. Because $H19^{+/hIC1}$ embryos display similar phenotypes to those of many patients with SRS who present with IC1 hypomethylation, including altered *H19* and *Igf2* expression and growth defects (23, 24), we hypothesized that these embryos can serve as a model for SRS. Placental growth defects are prevalent among individuals with SRS (24); thus, we further characterized $H19^{+/hIC1}$ placentas to study potential mechanisms underlying SRS associated with IC1 hypomethylation. We performed histological analyses on E15.5 $H19^{+/hIC1}$ placentas to explore whether abnormal placentation could contribute to embryonic growth restriction, given that *H19* and *Igf2* play essential roles in placental development (25, 26). In addition to being smaller (~74% of $H19^{+/+}$), $H19^{+/hIC1}$ placentas displayed an increased junctional/labyrinthine zone ratio, indicative of abnormal placenta morphology (Fig. S2 *G* and *H*).

Discussion

Using a mouse model replacing endogenous mIC1 with hIC1, we have shown that the ability of hIC1 to functionally replace mIC1 depends on the parental origin of the hIC1 allele. Although the main aim of this study was to investigate interspecies compatibility of hIC1 in the mouse system, we anticipate that findings from this study also will provide insight into modeling and further examining imprinting disorders such as BWS and SRS.

Several groups have reported that a subset of patients with BWS carry mutations at IC1, and that these mutations are largely associated with IC1 hypermethylation, reduced *H19* expression, and biallelic *Igf2* expression. Notably, these IC1 mutations (i.e., microdeletions and point mutations) manifest BWS clinical phenotypes when the mutant allele is maternal in origin (9, 27, 28). Determining the extent to which these mutations contribute to the molecular and clinical phenotypes of BWS is challenging, because IC1 hypermethylation is mosaic in the patients, suggesting that not all cells are aberrantly DNA-methylated. Moreover, clinical phenotypes of the patients are highly variable, possibly as a consequence of either the mosaicism or the genetic background of the individuals (27). In this study, we have shown that maternal transmission of hIC1 can functionally replace mIC1 by properly regulating imprinted expression and hIC1 methylation. Thus, our findings raise the exciting possibility of modeling IC1 mutations associated with BWS in mice via maternal transmission.

In contrast, paternal transmission of hIC1 leads to loss of *H19* and *Igf2* imprinting; *H19* displays biallelic and increased expression, and *Igf2* is silenced. Offspring inheriting hIC1 paternally also exhibit severe growth restriction. Of note, previous studies have shown that *Igf2* null neonates are born smaller but viable (29, 30), suggesting that prenatal lethality of $H19^{+/hIC1}$ is not due solely to the loss of *Igf2*. Mice from two independent *H19* knockout models exhibited overgrowth, suggesting a growth-suppressing role of *H19* (31, 32). In addition, ectopic expression of *H19* caused late-gestation lethality (33). Thus, changes in both *H19* and *Igf2* may synergistically contribute to the severe growth restriction and prenatal lethality of $H19^{+/hIC1}$.

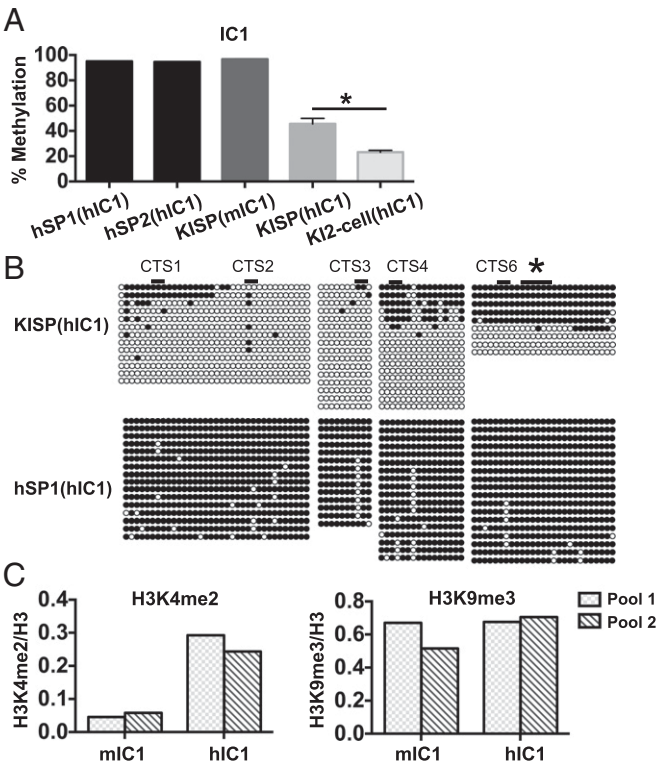

Fig. 4. Incomplete establishment of imprinting at the hIC1 in knock-in male germ cells. (*A*) Percent methylation at IC1 measured by pyrosequencing; assays *d* and *l* were used (Fig. 1*C*). From left to right, results for endogenous hIC1 in mature sperm samples from fertile men (hSP1 and hSP2), the endogenous mIC1 and targeted hIC1 in knock-in sperm (KISP) from adult mice, and the targeted hIC1 in pools of $H19^{+/hIC1}$ two-cell stage embryos (KI2 cells) are shown. KISP, $n = 6$ mice; KI2 cell pools, $n = 3$. $^*P < 0.05$, two-tailed Student's *t* test with equal variance. Bars represent mean ± SEM; error bar of the KISP (mIC1) is too small to be seen on the graph. (*B*) Methylation at hIC1 in KISP and hSP1 analyzed by bisulfite treatment followed by sequencing. Assays *e*–*h* were used (Fig. 1*C*). Cytosines in CG dinucleotides that are conserved between mouse and human and located within CTS are depicted as black lines above the clones and marked as CTS1, 2, 3, 4, and 6 (13). Cytosines measured by pyrosequencing are marked with an asterisk. (*C*) ChIP–qRT-PCR for H3K4me2 and H3K9me3 at mIC1 and hIC1 in knock-in round spermatids. Assays *b* and *j* were used (Fig. 1*C*). Two independent pools of round spermatids were generated as detailed in *Materials and Methods*, and the results from each pool are shown separately.

Previous studies have shown that abnormal *H19* and *Igf2* expression is linked to both placental and embryonic growth defects. Deletion of a placenta-specific *Igf2* transcript was found to result in growth restriction of embryos in late gestation (34). In a mouse model in which *H19* was deleted and *Igf2* expression was increased, both the placenta and the fetus were overgrown at E19 (35, 36). In humans, placental growth defects are common in individuals with BWS and SRS (24, 37). We observed that $H19^{+/hIC1}$ placentas not only are smaller, but also have abnormal placental morphology. Although the contribution of an abnormal placenta to fetal growth defects is unclear, it is noteworthy that *H19* is more highly expressed in the labyrinthine zone compared with the junctional zone (38), and that *Igf2* null mice display a disproportionate reduction in the labyrinthine zone compared with the junctional zone (39). These observations suggest a potential major growth-suppressing effect of increased *H19* and silenced *Igf2* expression in the labyrinthine zone.

We also have shown that hIC1 is partially methylated in the male germ line of $H19^{hIC1/+}$ mice. This phenotype is in contrast with that of other mouse models that carry mIC1 mutations; in those mice, methylation is properly established at nonmutated CpGs in the male germ line (5, 40). This finding suggests that interspecies communication between mouse and human is ineffective in establishing IC1 methylation. Based on our finding that hIC1 is abnormally enriched with activating H3K4me2 marks in the male germ cells, it is tempting to speculate that somatic histone modification marks carried from the maternal allele are not completely erased in the male germ cells. (Note that hIC1 was necessarily transmitted maternally to generate offspring.) Consequently, the establishment of DNA methylation at hIC1 is inhibited. This finding adds to the growing consensus that H3K4 methylation marks are inhibitory to de novo DNA methylation in the germ line, whereas repressive histone marks do not play major role in the establishment of methylation at ICRs (14, 16–18, 20). However, it is equally possible that the hypomethylated state of DNA attracts H3K4me2 at hIC1 by an unknown mechanism. More detailed time course analyses of DNA methylation and H3K4me2 enrichment in the primordial germ cells and early-stage male germ cells will provide insight into this hypothesis. Alternatively, there might be an inherent difference between mIC1 and hIC1 in terms of acquisition of methylation. A noncoding transcript has been detected at mIC1 during methylation acquisition in male germ cells (41), suggesting a potential role of transcription in the establishment of methylation at mIC1. Whether the same holds true at hIC1 remains to be determined, however.

Finally, we have shown that the partially established methylation at hIC1 in the male germ line is not properly maintained during preimplantation development. We also have shown that CTCF ectopically binds to hIC1 on the paternal allele in somatic cells. Similar results have been reported for an earlier mouse model in which CpGs within the CTCF-binding sites at the mIC1 were mutated to abrogate methylation, while keeping the CTCF-binding motifs intact (5). There, although methylation was properly established in the male germ cells at the mIC1, it was not maintained during preimplantation development (5). These data suggest that CTCF binding inhibits the maintenance of DNA methylation in somatic cells, although the mechanism remains unknown. Alternatively, hIC1 might lack properties that allow the mouse imprint maintenance machinery to properly recognize the sequence. It is also possible that hIC1 contains inhibitory signals that block accessibility and/or activity of the mouse imprint maintenance machinery.

In conclusion, we have elucidated hitherto unreported principals regarding the conservation of ICR function at the *H19*/*Igf2* locus and molecular mechanisms associated with SRS. First, evidence of incomplete histone reprogramming at hIC1 suggests that the mechanism regulating histone reprogramming at IC1 in the germ line has diverged between mouse and human. In this regard, it would be interesting to explore whether an IC1 ortholog of a species more closely related to mouse could recapitulate the wild-type epigenetic pattern on paternal transmission. Second, despite the fact that IC1 hypomethylation is the most common epimutation found in individuals with SRS (24), the molecular mechanism underlying the phenotype remains elusive. Obstacles to addressing this question include mosaicism of the epimutation in patients and the lack of a suitable genetic model system. We suggest that the paternal transmission of hIC1 in mice can be used to study the molecular mechanisms underlying SRS associated with IC1 hypomethylation. Future experiments, such as breeding $H19^{hIC1/+}$ males with *H19* null females, will help elucidate the extent to which *H19* contributes to the SRS-like phenotype. In addition, identifying pathways altered by IC1 hypomethylation may shed light on the physiology of SRS.

Materials and Methods

Targeting Vector. Detailed information on the hIC1 target vector is provided in *SI Materials and Methods*.

ES Cells and Mouse Generation, Breeding, and Genotyping. Details regarding ES cell targeting, Southern blot analyses, and mouse generation, breeding, and genotyping are provided in *SI Materials and Methods*.

Gene Expression Analysis. RNA isolation and cDNA synthesis was performed as described previously (42). For qRT-PCR, total expression levels of *H19* and *Igf2* were measured relative to the geometric mean of expression levels of *Arbp* (*acidic ribosomal phosphoprotein P0*), *Nono* (*non–POU domain-containing, octamer-binding protein*), and *Rpl13a* (*ribosomal protein L13A*). For the *y*-axis on the graph, the mean value of wild-type is set arbitrarily as 1. Details are provided in *SI Materials and Methods*.

DNA Methylation Analysis. gDNA isolation from neonatal, embryonic, and germ cell samples; bisulfite treatment; and methylation analyses are described in detail in *SI Materials and Methods*.

Histology. Histological analysis was performed as described previously (43).

Mouse Spermatogenic Cell Fractionation. Round spermatid fractions of mouse spermatogenic cells were collected using STA-PUT in two independent replicates, and the purity of each fraction was verified as described previously (22, 44). Each collection used both testes of 12 heterozygous ($H19^{hIC1/+}$) male mice. The purity was measured as 87% for pool 1 and 86% for pool 2.

Isolation of MEFs. MEFs were isolated from individual day 12.5 embryos in a B6 background as described previously (15).

ChIP–qRT-PCR Analysis. ChIP–qRT-PCR was carried out as described previously (44); details are provided in *SI Materials and Methods*. Each ChIP signal was calculated as the percent input of each immunoprecipitation (IP) normalized to nonspecific IgG (percent input of IP – percent input of IgG). In Fig. 4*C*, the *y*-axis denotes the ChIP signal of each histone mark normalized to that of total H3 (e.g., percent input of H3K4me2/percent input of total H3).

ACKNOWLEDGMENTS. This work was supported by US Public Health Service Grants GM51279 (to M.S.B.) and HD068157 (to M.S.B. and S.L.B.); Advanced Imaging Research Center Grant 8700 (to F.C.); Telethon-Italy Grant GGP15131 (to A.R.); European Union Seventh Framework Programme, INGENIUM 290123 (to A.R.); and National Institutes of Health Training Grant T32 GM07229 (to S.K.H.).

1. Lee JT, Bartolomei MS (2013) X-inactivation, imprinting, and long noncoding RNAs in health and disease. *Cell* 152(6):1308–1323.
2. Kalish JM, Jiang C, Bartolomei MS (2014) Epigenetics and imprinting in human disease. *Int J Dev Biol* 58(2-4):291–298.
3. Eggermann T, et al. (2015) Imprinting disorders: A group of congenital disorders with overlapping patterns of molecular changes affecting imprinted loci. *Clin Epigenetics* 7:123.
4. Ideraabdullah FY, Vigneau S, Bartolomei MS (2008) Genomic imprinting mechanisms in mammals. *Mutat Res* 647(1-2):77–85.
5. Engel N, West AG, Felsenfeld G, Bartolomei MS (2004) Antagonism between DNA hypermethylation and enhancer-blocking activity at the H19 DMD is uncovered by CpG mutations. *Nat Genet* 36(8):883–888.
6. Smits G, et al.; SAVOIR Consortium (2008) Conservation of the H19 noncoding RNA and H19-IGF2 imprinting mechanism in therians. *Nat Genet* 40(8):971–976.
7. Jinno Y, et al. (1996) Mouse/human sequence divergence in a region with a paternal-specific methylation imprint at the human H19 locus. *Hum Mol Genet* 5(8):1155–1161.
8. Jones BK, Levorse J, Tilghman SM (2002) A human H19 transgene exhibits impaired paternal-specific imprint acquisition and maintenance in mice. *Hum Mol Genet* 11(4):411–418.
9. Demars J, Gicquel C (2012) Epigenetic and genetic disturbance of the imprinted 11p15 region in Beckwith–Wiedemann and Silver–Russell syndromes. *Clin Genet* 81(4):350–361.
10. Engel N, Raval AK, Thorvaldsen JL, Bartolomei SM (2008) Three-dimensional conformation at the H19/Igf2 locus supports a model of enhancer tracking. *Hum Mol Genet* 17(19):3021–3029.
11. Nativio R, et al. (2011) Disruption of genomic neighbourhood at the imprinted IGF2-H19 locus in Beckwith–Wiedemann syndrome and Silver–Russell syndrome. *Hum Mol Genet* 20(7):1363–1374.
12. Mann MR, et al. (2003) Disruption of imprinted gene methylation and expression in cloned preimplantation stage mouse embryos. *Biol Reprod* 69(3):902–914.
13. Bell AC, Felsenfeld G (2000) Methylation of a CTCF-dependent boundary controls imprinted expression of the Igf2 gene. *Nature* 405(6785):482–485.
14. Delaval K, et al. (2007) Differential histone modifications mark mouse imprinting control regions during spermatogenesis. *EMBO J* 26(3):720–729.
15. Verona RI, Thorvaldsen JL, Reese KJ, Bartolomei MS (2008) The transcriptional status, but not the imprinting control region, determines allele-specific histone modifications at the imprinted H19 locus. *Mol Cell Biol* 28(1):71–82.
16. Lee DH, et al. (2010) CTCF-dependent chromatin bias constitutes transient epigenetic memory of the mother at the H19-Igf2 imprinting control region in prospermatogonia. *PLoS Genet* 6(11):e1001224.
17. Singh P, et al. (2013) De novo DNA methylation in the male germ line occurs by default but is excluded at sites of H3K4 methylation. *Cell Reports* 4(1):205–219.
18. Stewart KR, et al. (2015) Dynamic changes in histone modifications precede de novo DNA methylation in oocytes. *Genes Dev* 29(23):2449–2462.
19. Ooi SK, et al. (2007) DNMT3L connects unmethylated lysine 4 of histone H3 to de novo methylation of DNA. *Nature* 448(7154):714–717.
20. Ciccone DN, et al. (2009) KDM1B is a histone H3K4 demethylase required to establish maternal genomic imprints. *Nature* 461(7262):415–418.
21. Rose NR, Klose RJ (2014) Understanding the relationship between DNA methylation and histone lysine methylation. *Biochim Biophys Acta* 1839(12):1362–1372.
22. Bryant JM, Meyer-Ficca ML, Dang VM, Berger SL, Meyer RG (2013) Separation of spermatogenic cell types using STA-PUT velocity sedimentation. *J Vis Exp* (80):e50648.
23. Gicquel C, et al. (2005) Epimutation of the telomeric imprinting center region on chromosome 11p15 in Silver–Russell syndrome. *Nat Genet* 37(9):1003–1007.
24. Yamazawa K, et al. (2008) Molecular and clinical findings and their correlations in Silver–Russell syndrome: Implications for a positive role of IGF2 in growth determination and differential imprinting regulation of the IGF2-H19 domain in bodies and placentas. *J Mol Med (Berl)* 86(10):1171–1181.
25. Bartolomei MS, Ferguson-Smith AC (2011) Mammalian genomic imprinting. *Cold Spring Harb Perspect Biol* 3(7):a002592.
26. Reik W, et al. (2003) Regulation of supply and demand for maternal nutrients in mammals by imprinted genes. *J Physiol* 547(Pt 1):35–44.
27. Beygo J, et al. (2013) The molecular function and clinical phenotype of partial deletions of the IGF2/H19 imprinting control region depends on the spatial arrangement of the remaining CTCF-binding sites. *Hum Mol Genet* 22(3):544–557.
28. Abi Habib W, et al. (2014) Extensive investigation of the IGF2/H19 imprinting control region reveals novel OCT4/SOX2 binding site defects associated with specific methylation patterns in Beckwith–Wiedemann syndrome. *Hum Mol Genet* 23(21):5763–5773.
29. DeChiara TM, Efstratiadis A, Robertson EJ (1990) A growth-deficiency phenotype in heterozygous mice carrying an insulin-like growth factor II gene disrupted by targeting. *Nature* 345(6270):78–80.
30. Baker J, Liu J-P, Robertson EJ, Efstratiadis A (1993) Role of insulin-like growth factors in embryonic and postnatal growth. *Cell* 75(1):73–82.
31. Schmidt JV, Levorse JM, Tilghman SM (1999) Enhancer competition between H19 and Igf2 does not mediate their imprinting. *Proc Natl Acad Sci USA* 96(17):9733–9738.
32. Ripoche MA, Kress C, Poirier F, Dandolo L (1997) Deletion of the H19 transcription unit reveals the existence of a putative imprinting control element. *Genes Dev* 11(12):1596–1604.
33. Brunkow ME, Tilghman SM (1991) Ectopic expression of the H19 gene in mice causes prenatal lethality. *Genes Dev* 5(6):1092–1101.
34. Constância M, et al. (2002) Placental-specific IGF-II is a major modulator of placental and fetal growth. *Nature* 417(6892):945–948.
35. Leighton PA, Ingram RS, Eggenschwiler J, Efstratiadis A, Tilghman SM (1995) Disruption of imprinting caused by deletion of the H19 gene region in mice. *Nature* 375(6526):34–39.
36. Angiolini E, et al. (2011) Developmental adaptations to increased fetal nutrient demand in mouse genetic models of Igf2-mediated overgrowth. *FASEB J* 25(5):1737–1745.
37. Armes JE, et al. (2012) The placenta in Beckwith–Wiedemann syndrome: Genotype–phenotype associations, excessive extravillous trophoblast and placental mesenchymal dysplasia. *Pathology* 44(6):519–527.
38. Keniry A, et al. (2012) The H19 lincRNA is a developmental reservoir of miR-675 that suppresses growth and Igf1r. *Nat Cell Biol* 14(7):659–665.
39. Coan PM, et al. (2008) Disproportional effects of Igf2 knockout on placental morphology and diffusional exchange characteristics in the mouse. *J Physiol* 586(20):5023–5032.
40. Engel N, Thorvaldsen JL, Bartolomei MS (2006) CTCF-binding sites promote transcription initiation and prevent DNA methylation on the maternal allele at the imprinted H19/Igf2 locus. *Hum Mol Genet* 15(19):2945–2954.
41. Henckel A, Chebli K, Kota SK, Arnaud P, Feil R (2012) Transcription and histone methylation changes correlate with imprint acquisition in male germ cells. *EMBO J* 31(3):606–615.
42. de Waal E, et al. (2014) In vitro culture increases the frequency of stochastic epigenetic errors at imprinted genes in placental tissues from mouse concepti produced through assisted reproductive technologies. *Biol Reprod* 90(2):22.
43. de Waal E, et al. (2015) The cumulative effect of assisted reproduction procedures on placental development and epigenetic perturbations in a mouse model. *Hum Mol Genet* 24(24):6975–6985.
44. Bryant JM, et al. (2015) Characterization of BRD4 during mammalian postmeiotic sperm development. *Mol Cell Biol* 35(8):1433–1448.
45. Thorvaldsen JL, Mann MR, Nwoko O, Duran KL, Bartolomei MS (2002) Analysis of sequence upstream of the endogenous H19 gene reveals elements both essential and dispensable for imprinting. *Mol Cell Biol* 22(8):2450–2462.
46. Stadnick MP, et al. (1999) Role of a 461-bp G-rich repetitive element in H19 transgene imprinting. *Dev Genes Evol* 209(4):239–248.
47. Kühn R, Rajewsky K, Müller W (1991) Generation and analysis of interleukin-4–deficient mice. *Science* 254(5032):707–710.
48. Plasschaert RN, et al. (2014) CTCF binding site sequence differences are associated with unique regulatory and functional trends during embryonic stem cell differentiation. *Nucleic Acids Res* 42(2):774–789.
49. Weaver JR, et al. (2010) Domain-specific response of imprinted genes to reduced DNMT1. *Mol Cell Biol* 30(16):3916–3928.
50. Takai D, Gonzales FA, Tsai YC, Thayer MJ, Jones PA (2001) Large-scale mapping of methylcytosines in CTCF-binding sites in the human H19 promoter and aberrant hypomethylation in human bladder cancer. *Hum Mol Genet* 10(23):2619–2626.